Magnetic and magnetotransport properties of ZnxFe3-xO4-y thin films

Nathalie Jedrecy, Christian Hebert, J. Perriere, M. Nistor, E. Millon

Magnetic and magnetotransport properties of $Zn_xFe_{3-x}O_{4-y}$ thin films

N. Jedrecy,[1,2,a)] C. Hebert,[1,2] J. Perriere,[1,2] M. Nistor,[3] and E. Millon[4]
[1]*Sorbonne Universités, UPMC Univ Paris 06, UMR 7588, INSP, 4 Place Jussieu, F-75005 Paris, France*
[2]*CNRS, UMR 7588, INSP, 4 Place Jussieu, F-75005 Paris, France*
[3]*National Institute for Lasers, Plasma and Radiation Physics, L22 P.O. Box MG-36, 77125 Bucharest, Romania*
[4]*Univ. Orleans, UMR CNRS 7344, GREMI, 14 Rue Issoudun, F-45067 Orleans 2, France*

(Received 19 June 2014; accepted 19 November 2014; published online 2 December 2014)

We present a detailed magnetic and magnetotransport investigation of spinel zinc ferrite $Zn_xFe_{3-x}O_{4-y}$ ($0.1 \leq x \leq 0.6$) thin films grown by pulsed laser deposition on various substrates. The films are ranging from polycrystalline to (001)- or (111)-oriented. It is shown associating magnetic and resistivity measurements to x-ray and ion beam scattering analyses that the magnetic and electrical properties are tightly linked to the chemical composition and crystallinity/microstructure of the films, as they result from the choice of substrate and growth conditions. The use of oxidizing conditions (O_2 pressure $\approx 10^{-4}$–10^{-2} mbar) is highly detrimental to the crystalline quality and thus to the ferromagnetism. On the contrary, a partial O_2 pressure of 3×10^{-7} mbar combined to a growth temperature of 500 °C allows obtaining $Zn_xFe_{3-x}O_{4-y}$ films displaying very good ferromagnetic features. The SiO_2/Si substrates, promoting (111) growth without interfacial effects, lead to better film properties than Al_2O_3(0001), MgO(001), or $SrTiO_3$(001) substrates: higher Curie temperatures and higher magnetization values ($\approx$490 kAm^{-1}) at room temperature. Above a Verwey-type critical temperature, a thermally activated spin polarized charge transport is observed, while in the low temperature range, the resistivity is well described by the variable range hopping model. However, the negative magnetoresistance response at low field remains modest and a monotonous decrease with increasing magnetic field is observed. We show that a steeper low field magnetoresistance decrease may be obtained in polycrystalline stoichiometric layers formed by a specific two-step growth process, which significantly reduces the density of grain/antiphase boundaries. © *2014 AIP Publishing LLC*. [http://dx.doi.org/10.1063/1.4903211]

I. INTRODUCTION

Spinel oxides are considered as high potential materials for spintronics applications.[1–3] For instance, the archetype Fe_3O_4 spinel combines high Curie temperature with an optimal 100% theoretical value of the spin polarization.[4,5] Solid solution systems such as $Zn_xFe_{3-x}O_4$ ($0 \leq x \leq 1$) offer the possibility to tune the magnetic and charge transport properties as desired, from ferromagnetic to antiferromagnetic and from conducting to insulating.[6–9] They open the way to the design and fabrication of novel magnetic recording or microwave devices. However, spinel oxide inclusion in current device technology presupposes controlled growth in the form of thin films and compatibility/integration with conventional semiconductors like Si.[10–14]

A large number of studies exist concerning thin films of magnetite (Fe_3O_4). Antiphase boundaries (APBs) are considered as the main limitation to the saturation magnetization and to the electrical conductivity.[3,15–17] On the contrary, zinc ferrite $Zn_xFe_{3-x}O_4$ thin films ($x < 1$) have been scarcely investigated.[7,8,18,19] Magnetic and electronic properties of AB_2O_4 spinel oxides are determined by the cation distribution among particular tetrahedral (A) and octahedral (B) sites of the face centered cubic oxygen sublattice. In $Zn_xFe_{3-x}O_4$ zinc ferrites, the nonmagnetic ($3d^{10}$) Zn^{2+} cations occupy very preferentially the A sites,[20] leaving the remaining A and B sites to the iron ($3d^5/3d^6$) Fe^{3+}/Fe^{2+} cations. Due to the higher energy stabilization by the crystal field of $3d^6$ ions in B sites with respect to A sites and equivalency of the two types of sites for $3d^5$ ions, the zinc ferrite formula is expected to be

$$(Zn^{2+}{}_xFe^{3+}{}_{1-x})_A(Fe^{3+}{}_{1+x}Fe^{2+}{}_{1-x})_BO^{2-}{}_4. \quad (1)$$

The lattice parameter related to 8 $Zn_xFe_{3-x}O_4$ units ranges from 8.395 Å ($x = 0$) to 8.43 Å ($x = 1$). Owing to the strong and dominant antiferromagnetic (AF) coupling between the A and B sites in spinel structures, the magnetic moments in the B sites are expected to be parallel to each other. The spin only magnetic moment of a Fe^{3+} (Fe^{2+}) ion being 5 (4) μ_B, where μ_B is the Bohr magneton, the magnetic moment per $Zn_xFe_{3-x}O_4$ formula unit (f.u.) is, thus, theoretically equal to $m = (4 + 6x)\ \mu_B$. Nevertheless, this formula is no more valid for $x \geq 0.5$ because of the decrease (increase) of A-B (B) AF interactions when the number of magnetic moments in A sites decreases.[7,21] Ferromagnetically aligned Fe^{2+} and Fe^{3+} ions in B sites allow charge transport involving (minority) single spin state t_{2g} electrons.

In this work, the structural, magnetic, and magnetotransport properties of $Zn_xFe_{3-x}O_{4-y}$ films ($0.1 \leq x \leq 0.6$ and $0 \leq y \leq 0.4$) grown using different oxygen partial pressures, temperatures, and substrates, are reported and discussed. The physical properties are directly linked to the crystallinity/microstructure and chemical composition of the

a)jedrecy@insp.jussieu.fr

films, including their non stoichiometry (i.e., the presence of oxygen or iron vacancies).

II. EXPERIMENTAL

The films were grown on $Al_2O_3(0001)$, MgO(001), $SrTiO_3(001)$, and SiO_2-covered Si(001) crystals by pulsed laser deposition (PLD) from stoichiometric $Zn_xFe_{3-x}O_4$ targets ($0.1 \leq x \leq 0.6$). We used a frequency quadrupled (266 nm) Nd:YAG laser with 7 ns duration pulses at a 10 Hz repetition rate. Note the orientation of the Si substrate is here not meaningful since our crystals were terminated by a thin ($\sim$2 nm) amorphous SiO_2 layer. The targets were prepared by mixing powders of the precursor ZnO and Fe_2O_3 oxides to obtain the desired Zn/Fe proportion, followed by a sintering treatment at 1000 °C. The films chemical composition and thickness were determined quantitatively by using the most accurate and adapted method for this purpose, the random Rutherford backscattering spectrometry (RBS) ion analysis. The thicknesses investigated range from 70 to 150 nm. X-ray diffraction (XRD) measurements were carried out with Cu K_α radiation using a 4- or 6-circle diffractometer. Cross-section transmission electron microscopy (TEM) was performed with a JEOL apparatus. The magnetic and DC transport (in four Au/Al bars geometry) properties were measured with a Physical Property Measurement System (PPMS) including Vibratometer Sample Magnetometer (VSM). All samples used with the VSM were, furthermore, analyzed by RBS to ensure the accurateness of the magnetization values and chemical compositions given in this paper.

III. RESULTS AND DISCUSSION

The $Zn_xFe_{3-x}O_4$ crystallization in the AB_2O_4 spinel structure requires using growth or annealing temperatures of $\approx$450–500 °C. Lower temperatures lead to inhomogeneous films with small ZnO crystallites. Keeping fixed the substrate temperature at 500 °C, the use of high O_2 pressure (10^{-2} mbar) leads to low crystalline quality spinel films without preferential orientation of the grains, whereas a 3×10^{-7} mbar O_2 pressure ensures the growth of high crystalline quality substrate-normal single oriented spinel films. Well defined *hhh* (*00l*) spinel peaks in the x-ray diagrams are obtained on SiO_2/Si and Al_2O_3 (MgO and $SrTiO_3$) in accordance with a (111) ((001)) film orientation. A typical θ-2θ scan from a (111) zinc ferrite film grown on SiO_2/Si is shown in Fig. 1(a). The cubic lattice parameter of the $x = 0.33$ spinel film is found equal to 8. 405 Å, in perfect accordance with the value calculated from bulk Fe_3O_4 to $ZnFe_2O_4$ lattice parameters. The *440* pole figure measurement attests that there is no in-plane preferential azimuthal orientation on SiO_2/Si. The growth on Al_2O_3 leads to (111) epitaxial films with the azimuthal in-plane $\langle 110\rangle // \langle 210\rangle_{Al2O3}$ orientation. A different type of film was elaborated using a two-step process: first, an amorphous film was grown at room temperature (RT) under 3×10^{-7} mbar O_2, second, the film was *in situ* annealed at 450 °C ($\sim$1 h 30 min, same O_2 pressure). The resulting film exhibits a high quality polycrystalline form (see Fig. 1(a)), with a width of the x-ray peaks comparable to that of the textured (e.g., (111) on SiO_2/Si) or epitaxial form (e.g., (111) on Al_2O_3).

Figure 1(b) displays the two RBS profiles obtained from the high quality, respectively (111)-oriented and polycrystalline, spinel films grown on SiO_2/Si ($P_{O2} = 3 \times 10^{-7}$ mbar in both cases, growth temperature of 500 °C in the first case, RT growth and annealing in the second case). The RBS fits were done using the program RUMP. Whereas the chemical composition of the (111) film is homogeneous and equal to $Zn_{0.33}Fe_{2.67}O_{3.9}$ over the whole 86 nm thickness, the polycrystalline film reveals three regions (see Figs. 1(c) and 1(d)). Starting from the interface, the composition evolves from $Zn_{0.93}Fe_{2.07}O_{3.0}$ over the first 54 nm, then to $Zn_{0.45}Fe_{2.55}O_4$ over the second 50 nm, and finally to $Zn_{0.33}Fe_{2.67}O_4$ over the last 44 nm. This in-depth Zn/Fe/O concentration profile results from the two-step growth process and it may nicely be explained as follows. We consider as a starting point, a non stoichiometric amorphous $Zn_xFe_{3-x}O_{4-y}$ film at RT. The annealing leads to an inhomogeneous repartition of the Zn (and Fe) cations as well as of the O anions. Two thirds of the thickness of the film close to the surface transform into Zn-depleted (Fe-enriched) fully stoichiometric $Zn_{x-z}Fe_{3-x+z}O_4$ layers, while one third close to the interface transforms into a Zn-enriched (Fe-depleted) strongly oxygen deficient $Zn_{x+2z}Fe_{3-x-2z}O_{4-3y}$ zone. The RBS-derived compositions, close to $Zn_{0.99}Fe_{2.20}O_{3.19}$ for one third of the thickness towards the interface and on average about $Zn_{0.39}Fe_{2.61}O_4$ for the two remaining thirds towards the surface, are fully consistent with such an evolution taking $x = 0.59$, $y = 0.27$, $z = 0.20$. The Zn enrichment of the layers close to the interface has driven their oxygen depletion, in favor of the remaining film, which becomes Fe-enriched and stoichiometric in oxygen. The new species repartition across the film thickness as induced by the solid phase crystallization of the two-step process has been retrieved using other substrates and/or different amounts of deposited material. For instance on Al_2O_3, a 100 nm thick film leads to a 50 nm thick $Zn_{x+2z}Fe_{3-x-2z}O_{4-3y}$ interface region and a 50 nm thick surface $Zn_{x-z}Fe_{3-x+z}O_4$ region, where $x = 0.387$, $y = 0.133$, and $z = 0.057$. It is important to note that the RT-annealed polycrystalline films are very dense (not granular) films with surface smoothness comparable to that of the (111)-oriented films. Cross section TEM images of the as-grown (111)-oriented and polycrystalline RT-annealed films on SiO_2/Si are shown in Figs. 1(e) and 1(f), respectively. One may note that only for the (111) film, irregularly spaced abrupt APBs are observed, generating strain inside the Si substrate.

The magnetization M of the high quality $Zn_{0.33}Fe_{2.67}O_{3.9}$ (111) film, measured at 300 K as a function of an external magnetic field μ_0 H, applied either in the surface plane (IP) or out of the surface plane (OP), is shown in Fig. 2(a). First, the magnetization at saturation M_s reaches $\sim$490 kAm^{-1}, a value which corresponds to 3.93 μ_B per f.u. The M-H measurement at 10 K leads to $M_s \sim 601$ kAm^{-1} that is 4.81 μ_B per f.u. Considering a

$$(Zn^{2+}{}_xFe^{3+}{}_{1-x})_A(Fe^{3+}{}_{1+x-2y}Fe^{2+}{}_{1-x+2y})_BO^{2-}{}_{4-y} \qquad (2)$$

ion repartition, where $x = 0.33$ and $y = 0.1$, the measured saturation magnetization amounts to 83% of the theoretical

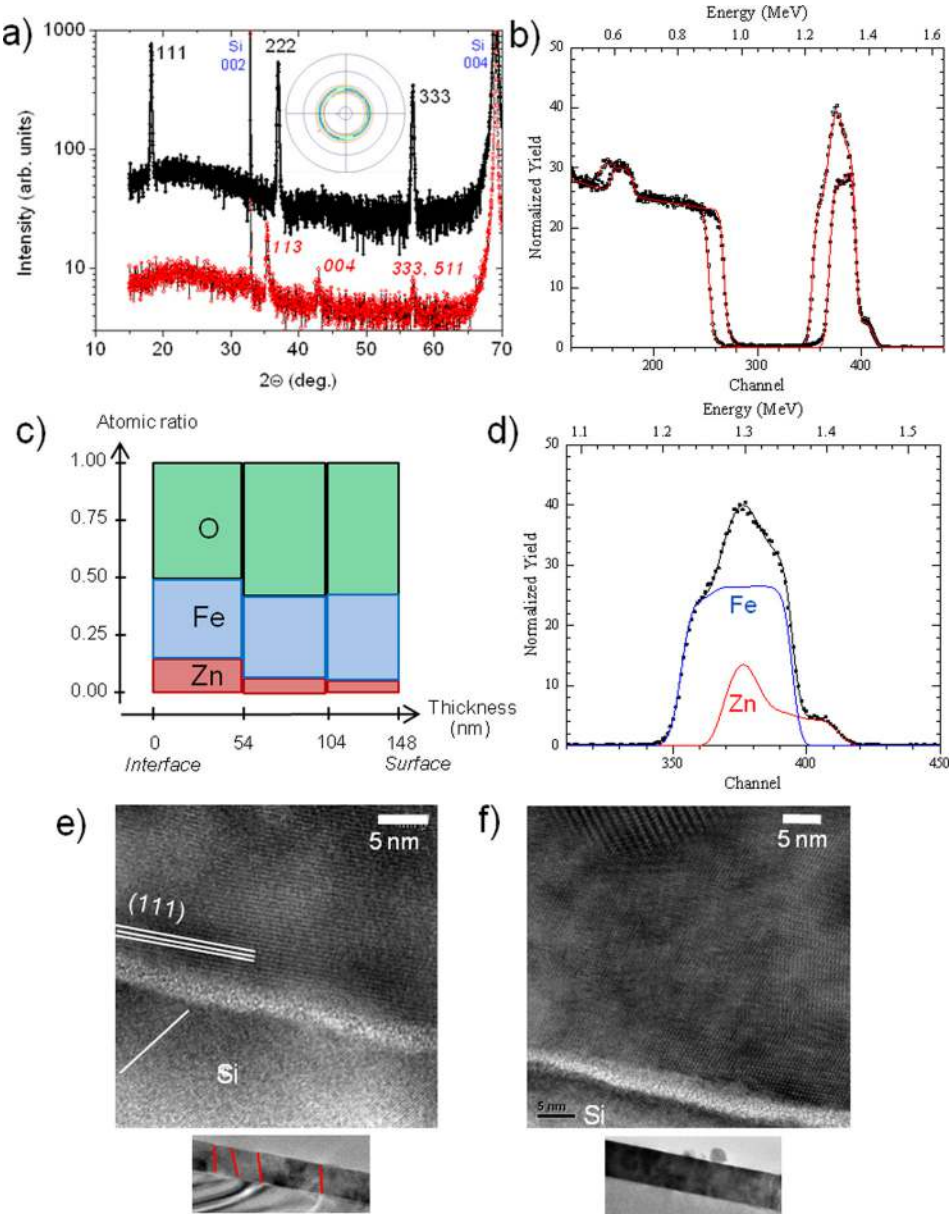

FIG. 1. (a) θ–2θ scans from high crystalline quality (111)-oriented and polycrystalline $Zn_xFe_{3-x}O_{4-y}$ spinel films grown on SiO_2/Si. The 440 pole figure of the (111) film is shown as an inset. (b) Corresponding RBS profiles. (c) Concentration profile of the atomic species in the RT-annealed polycrystalline film. (d) Decomposition of the RBS profile. (e) and (f) TEM images from the high quality (111)-oriented and polycrystalline films, respectively. The APBs of the (111) film (left down image) are indicated.

moment $m^{theor.} = (4 + 6x - y)\ \mu_B = 5.78\ \mu_B$. For comparison, the best value reported for Fe_3O_4 films is 70% of the theoretical expectation.[3] Second, a very high remanent magnetization M_r value is obtained in the IP configuration ($M_{r\_IP} = 0.80\ M_s$) associated to a small coercitive field ($\mu_0 H_{c\_IP} = 18$ mT at 300 K). In the OP configuration, the saturation is reached for a moderate field of 1 T and the remanent magnetization is reasonably high ($M_{r\_OP} = 0.08\ M_s$), considering the fact that magnetization alignment along the normal needs to overcome the thin film shape anisotropy. This behavior may be related to the magnetocrystalline anisotropy of the (111) spinel film, with the normal being an easy magnetization axis.

Surprisingly, the polycrystalline film grown at RT and annealed at 450 °C gives very good magnetic properties too. Considering that about one third of that film (close to the interface) has a composition close to 1 ZnO and 2.2 FeO which are by nature non magnetic and AF, respectively, the M_s value must be evaluated reducing the thickness of the film to its active ferrimagnetic part (2/3 of the total thickness). Under this assumption, one obtains $M_s = 522$ kAm^{-1} at 300 K and $M_s = 612$ kAm^{-1} at 10 K (see Table I for the uncorrected values), with $M_{r\_IP} = 0.50\ M_s$. Noticeably, the AF region at the interface is revealed by the shift of the M-H hysteresis at 10 K (see Fig. 2(b)), with an exchange field of about 10 mT.

The magnetic results of other representative films are summarized and sorted by decreasing M_s values at 300 K in Table I. Interestingly, there is no enhancement of the magnetic properties of the (111) epitaxial film on Al_2O_3(0001) with respect to the (111) films on SiO_2/Si constituted by domains with random in-plane orientations. As for films which proved of poor crystalline quality, the M_s values are noticeably low. Figure 3(a) displays the dependence of M_s derived from M-H curves as a function of the temperature T for a series of spinel films all grown at 500 °C but with different O_2 pressures. All experimental $M_s(T)$ values are in nice accordance with the Bloch law: $M_s(T)/M_s(0) = [1 - (T/T_c)^{3/2}]$, where T_c is the

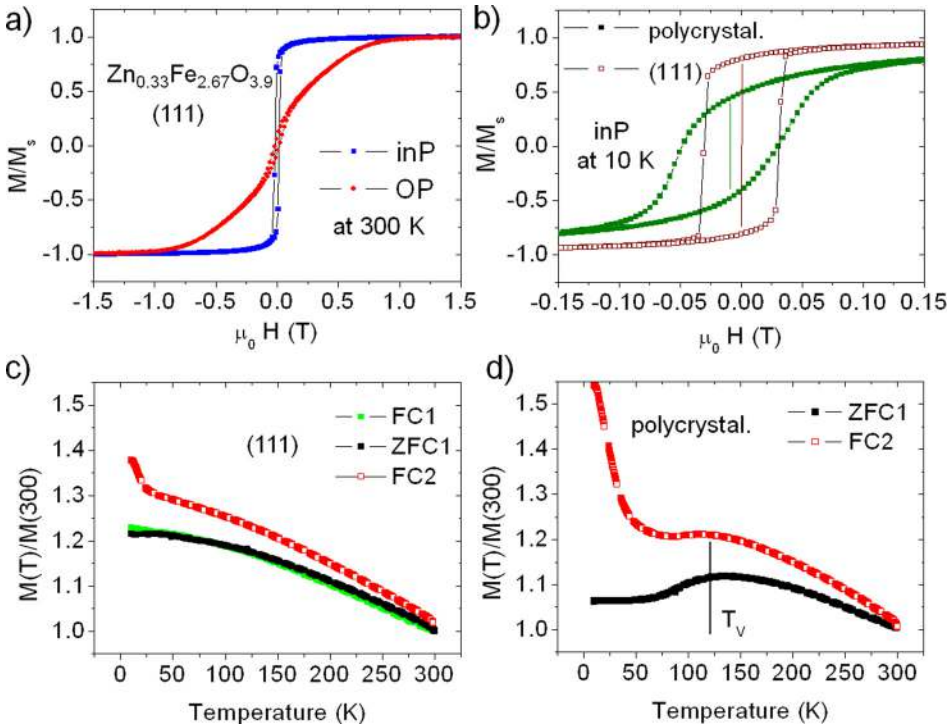

FIG. 2. (a) M-H hysteresis curves measured at 300 K of a (111) spinel film grown on SiO_2/Si in the in-plane (inP) and out-of-plane (OP) configurations. The M_s saturation value is worth 490 kAm^{-1}. (b) InP M-H curves (low field region) at 10 K from high crystalline quality (111)-oriented and polycrystalline films. The M_s value for the (111) film is 600 kAm^{-1}. (c) and (d) Magnetization as a function of temperature from the (111) and polycrystalline films, respectively (see text for the definition of the ZFC1, FC1, and FC2 curves).

Curie temperature. This attests that the magnetic properties arise from homogeneous ferromagnetic layers. However, the films grown at 10^{-4} or 10^{-2} mbar O_2 give $T_c \leq 480$ K, while those grown under 3×10^{-7} mbar O_2 (except the film grown on $SrTiO_3$) give T_c close to 860 K, the Curie temperature of bulk magnetite. The (001) film obtained on $SrTiO_3$ as well as that on MgO have a specific chemical composition (see Table I). Stoichiometric layers (no oxygen vacancies) are formed on $SrTiO_3$ and near the interface with MgO. The $SrTiO_3$ oxide obviously acts as an oxygen reservoir during the film crystallization, resulting in a low T_c value. The effects are less pronounced with MgO, where only the interface region is oxygen rich. Therefore, both the substrate and the O_2 pressure conditions have a strong impact on the T_c value, a low T_c value being associated to enhanced changes with temperature of the coercitive field H_c and of the ratio M_r/M_s (see Fig. 3(b)). Finally, three groups of zinc ferrite films may be distinguished: the first group is constituted by the high crystalline quality (111)-oriented or polycrystalline films (m^{10K} moment per f.u. at 10 K on average about 77% of the m^{theor} theoretical value), the second group is constituted by the high crystalline quality (001)-oriented films ($m^{10K} \approx 58\%$ m^{theor}), the third group is constituted by the low crystalline quality films ($m^{10K} \approx 26\%$ m^{theor}). An O_2-rich environment during the zinc ferrite film growth is detrimental to the crystalline order and to the ferromagnetism. However, high quality fully oxygen-stoichiometric polycrystalline layers (no oxygen vacancies) that lead to optimal ferromagnetic features may be obtained by using the two-step process.

We discuss in the following the possible reasons for the mediocre M_s and T_c values of the films grown in excess of oxygen. The composition of the film grown at 10^{-2} mbar O_2 interestingly reveals that cation sites are unoccupied. In an ideal scheme, one iron vacancy (□) is expected to be created concomitantly to the oxidation of three Fe^{2+} into two Fe^{3+} ions.[22] In Fe_3O_4, this oxidation process leads to the $Fe_{3-\delta}O_4$ spinel form, where magnetization may be reduced from 4 to 3.3 μ_B per f.u. evolving from magnetite ($\delta = 0$) to maghemite γ-Fe_2O_3 ($\delta = 1/3$) phase under assumption of a preserved spinel-derived ordered structure. In our case, the iron vacancies cannot explain by themselves the M_s value measured at 10 K, far lower than expected. Indeed, under assumption of a cation ordered repartition, one should obtain 6.8 μ_B per $Zn_{0.51}Fe_{2.34}$ $\square_{0.15}O_4$ f.u. instead of the 1.5 μ_B experimental value. The main reason the M_s and T_c values of the films grown under 10^{-2} mbar O_2 are so low is thus the disorder introduced by the oxygen in excess during the growth process and which results in poorly crystallized layers. For having confirmation of this effect, we have annealed in air (~48 h) some films grown at 500 °C under 10^{-7} mbar O_2. Whereas the composition of the films is logically found evolving from $Zn_xFe_{3-x}O_{4-y}$ to $Zn_xFe_{3-x}O_4$, the M_s value is found divided by a factor 10. Such a large reduction of the magnetization confirms that the oxidation process not only modifies the Fe^{3+}/Fe^{2+} ratio accordingly to the number of annihilated oxygen vacancies. The primary disruptive factor of the ferrimagnetic order between cations is the strong structural disorder induced by the incorporation of oxygen atoms in the spinel lattice.

We have compared the zero-field cooled (ZFC) and field-cooled (FC) magnetizations as a function of the temperature of the high quality (111) and polycrystalline films grown at 10^{-7} mbar O_2 on SiO_2/Si. Although the two types of films were showing the same $M_s(T)$ dependence (see Fig. 3(a)), they display very different M(T) behaviors (see Figs. 2(c) and 2(d)). After cooling the samples from RT to 10 K without magnetic field, the ZFC data, labeled as ZFC1, were recorded during warming, applying a small magnetic field ($\mu_0 H = 5$–10 mT). The FC1 (FC2) data were recorded during cooling (warming) with the same H (after prior

TABLE I. Summary of the in-plane magnetic properties of spinel films grown under different conditions.

Substrate	Growth temperature (°C)	O_2 pressure (mbar)	Film composition	Film orientation	M_s at 300 K = $M_s(300)$ (kA m^{-1})	Mr/Ms at 300 K	M_s at 10 K = $M_s(10)$ (kA m^{-1})	m_r/f.u. at 300 K (μ_B)	m_r/f.u. at 10 K (μ_B)	$m^{10K}/m^{theor.}$ (%)
SiO_2/Si	RT + anneal. 450	3×10^{-7}	$^1/_3$ $Zn_{0.33}Fe_{2.67}O_4$ (surf.) $^1/_3$ $Zn_{0.45}Fe_{2.55}O_4$ $^1/_3$ $Zn_{0.93}Fe_{2.07}O_{3.0}$ (int.)	High quality polycrystal	365.6 (uncor.) 522.4 (cor.)	0.5	428.8 (uncor.) 612.4 (cor.)	4.2	4.9	77
SiO_2/Si	500	3×10^{-7}	$Zn_{0.33}Fe_{2.67}O_{3.9}$	(111)	489.4	0.8	600.7	3.9	4.8	83
SiO_2/Si	500	3×10^{-7}	$Zn_{0.45}Fe_{2.55}O_{3.6}$	(111)	411.2	0.55	500.1	3.3	4.0	68
Al_2O_3 (0001)	500	3×10^{-7}	$Zn_{0.33}Fe_{2.67}O_{3.75}$	(111)	383.5	0.36	500.2	3.1	4.0	73
SiO_2/Si	500	3×10^{-7}	$Zn_{0.1}Fe_{2.9}O_{3.6}$	(111)	358.4	0.64	403.0	2.9	3.2	85
MgO (001)	500	3×10^{-7}	$^1/_2$ $Zn_{0.54}Fe_{2.46}O_{3.6}$ (surf.) $^1/_2$ $Zn_{0.3}Fe_{2.7}O_4$ (int.)	(001)	338.4	0.2	458.6	2.7	3.7	60
$SrTiO_3$ (001)	500	3×10^{-7}	$Zn_{0.6}Fe_{2.4}O_4$	(001)	306.2	0.37	540.1	2.5	4.3	57
SiO_2/Si	500	1×10^{-4}	$Zn_{0.5}Fe_{2.5}O_{3.8}$	Low quality	118.1	0.13	246.0	0.9	2.0	30
SiO_2/Si	500	1×10^{-2}	$Zn_{0.51}Fe_{2.34}\square_{0.15}O_4$	polycrystal	75.6	0	186.3	0.6	1.5	22
SiO_2/Si	350	3×10^{-7}	$Zn_{0.54}O_{0.54}/Fe_{2.45}O_{2.55}$	No spinel	8.7	0.36	…	0.1	…	…

cooling from 300 to 10 K under saturation for FC2). The FC2 data investigate the remanent magnetization. As expected from homogeneous layers without clusters, the ZFC1 and FC1 curves are nearly identical. For the (111) film, the ZFC1 and FC2 curves follow a similar monotonous decrease with raising T, while for the polycrystalline film, a local maximum is observed in the two types of curves at a temperature close to that of the Fe_3O_4 Verwey transition ($T_V = 120$ K). This local maximum still may be identified raising $\mu_0 H$ up to 100 mT. The ZFC1 curve of the polycrystalline film does not evolve anymore for $T < 75$ K; the steep increase of the FC2 curve for $T < 60$ K should be related to the $\langle 111 \rangle$ easy axes distribution. In high (low) quality epitaxial magnetite films, the Verwey transition manifests itself by an abrupt (smooth) change of the magnetization.[15,23] The presence of zinc in the $Zn_xFe_{3-x}O_4$ layers is expected to minimize/suppress this transition. Yet, a remnant of this transition occurs in the case of the RT-annealed polycrystalline film, differently than the as-grown (111)-oriented film. The transition temperature can hardly be associated to a T_B blocking temperature of nanosized grains since the polycrystalline film does not behave as superparamagnetic for $T > T_B$. Instead, we have a clear ferromagnetic behavior with $T_c > 860$ K; the ratio M_r/M_s as well as the coercitive field H_c are quasi-constant in the 10–300 K temperature range (see Fig. 3(b)). In magnetite, an ordered state of the cations in the B sublattice sets in below $T_V = 120$ K.[4] The APBs by being the place of AF interactions are known to alter this long range ferrimagnetic order of the magnetic moments.[15–17] From TEM analysis, such APBs are only revealed in the (111) film. Noticeably, the polycrystalline film is constituted by variously oriented domains without APBs and it does exhibit a Verwey-type transition in the magnetic behavior, contrary to the (111) film. This strongly suggests that the APBs would be the main limitation to charge/moment ordering and that polycrystalline films with a reduced density of APBs may be obtained using the two-step growth process.

Last, we discuss in the following the magnetotransport properties of the $Zn_xFe_{3-x}O_{4-y}$ films ($0.33 \leq x \leq 0.45$) grown at 10^{-7} mbar O_2 pressure, either at RT with post-annealing at 450 °C (polycrystalline form) or directly at 500 °C (single oriented form). All samples give similar variation of the resistivity ρ as a function of the temperature T. This is demonstrated in Fig. 4(a), where the resistivity of three different films grown on either MgO or Al_2O_3 is displayed in log scale as a function of (1/T). Measurements performed using a semi-insulating Si substrate led to similar results. The ρ values at 300 K are between 2 and 4.5×10^{-2} Ωcm, in accordance with the literature.[7,8] It is interesting to note that the resistivity at RT of the polycrystalline film is lower than that of the as-grown single-oriented film, confirming the lowest density of grain boundaries generated by the two-step growth process. The ρ(T) data in the high-temperature [$T_{lim.}$, 300 K] range may nicely be fitted with the function

$$\rho = \rho_0 \exp(E_a/k_B T), \tag{3}$$

where E_a has the meaning of a charge activation energy allowing for the hopping of electrons between the Fe^{2+} and

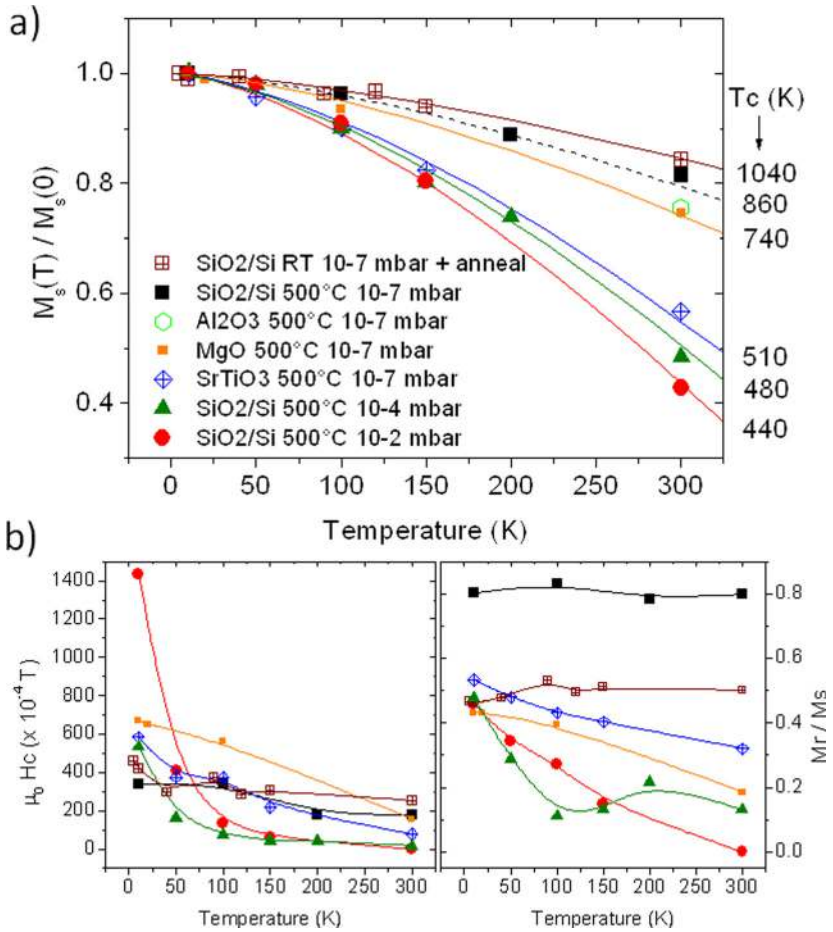

FIG. 3. (a) Saturation magnetization as a function of temperature for films grown under different conditions on different substrates. (b) Corresponding coercitive field and remanent over saturation magnetization ratio as a function of temperature.

Fe^{3+} cations in the B sites of the zinc ferrite spinel. The $T_{lim.}$ limit temperature corresponds to the Verwey-type temperature and it varies from 95 to 125 K depending on the sample. The three fits give $E_a = 62$ meV for the RT sample and 51 (57) meV for the sample grown at 500 °C on MgO (Al_2O_3). In the low-temperature [55 K, $T_{lim.}$] range, the data are fitted with the Mott's variable range hopping (VRH) model, where

$$\rho = \rho_0 \exp[(T_0/T)^{1/4}] \quad (4)$$

with T_0 varying from 1×10^8 to 3.8×10^7 K. It may be noted that the Verwey-type transition is easily identified in the resistivity curves from all zinc ferrite samples, while it is observed on the remanent M(T) curve from the high quality polycrystalline film alone. Indeed, in global magnetic measurements, the whole film contributes to the magnetic signal, while selective charge transport paths may dominate the signal in electrical measurements.

Figure 4(b) shows the magnetoresistance (MR) as a function of the field $\mu_0 H$

$$MR(H) = [R(H) - R(0)]/R(0) \quad (5)$$

from the single oriented and polycrystalline $Zn_xFe_{3-x}O_{4-y}$ films, respectively. The magnetic field H was applied perpendicular to the film plane. The MR(H) curves from the (111) film are very similar, in shape and in magnitude, to those already reported for epitaxial (001) $Zn_xFe_{3-x}O_4$ layers grown on MgO.[7] The data from the polycrystalline film are distinctly different, showing first a pronounced decrease of the MR in the [−1 T, 1 T] range and second, a change of the temperature dependence of MR(H) close to the Verwey-type temperature (∼100 K). The large high field values (≈−10%) and the linearity with H of MR(H) from the (111) film are predominantly related to spin-disorder scattering at the grain boundaries.[23,24] On the contrary, for the polycrystalline film, the enhanced MR response at low field and the near constant value of MR(H) at high field are suggestive of an enhanced spin-polarized tunneling between grains[25] (across grain boundaries) and/or of a lower density of grain boundaries such as APBs.[26] The magnetization of the grain boundaries is hardly detected in the global magnetic measurements due to their small volume fraction. For instance, the magnetic signal of the (111) film shown in Fig. 2(a) is mainly due to the alignment of the magnetic moments inside the different domains and the saturation state of these domains is almost reached for a field as low as 0.03 T. Differently, the very small magnetic signal from grain boundaries still rises continuously with increasing field up to a magnitude larger than 9 T. This grain boundary contribution, although negligible looking at the overall magnetization, clearly manifests itself in the resistivity measurements since charge transport necessarily involves conduction paths across or through the grain/antiphase boundaries. We know from the resistivity values and the TEM analysis that the boundaries between the crystallized grains in our RT-annealed polycrystalline film are extremely thin. As suggested from the M(T) curves, these

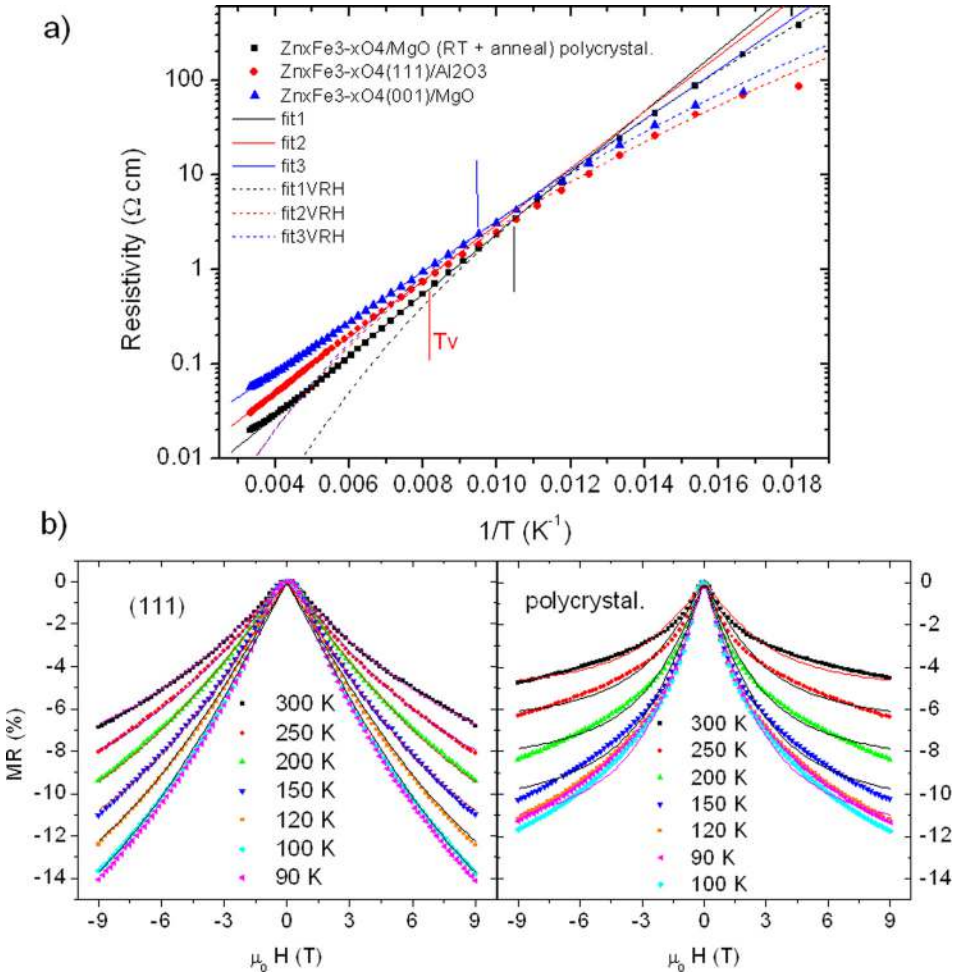

FIG. 4. (a) Resistivity in Log scale as a function of inverse of temperature for different films, together with appropriate fits using the thermal activated or VRH transport models. (b) Magnetoresistance data (with their fits) at different temperatures as a function of the OP magnetic field, for high crystalline quality (111)-oriented and polycrystalline films, respectively.

boundaries seem of different natures than the APBs, which couple antiferromagnetically adjacent domains. This specificity could explain the differences in the MR behavior, with respect to the single-oriented films. In order to quantify the MR changes between the two types of samples, the MR(H) curves were fitted on the basis of the function (3), assuming a field dependent $E_a(H)$ activation energy. This consists to consider that the hopping of spin down electrons between Fe^{2+} and Fe^{3+} ions in B sites is easiest when a magnetic field is applied, in other words, when a maximum of magnetic moments in B sites are parallel (//) to each other. The difference $\Delta E_a(H) = E_a(0) - E_a(H)$ is expected to be small since saturation is obtained with moderate magnetic fields, even in the OP configuration. We, thus, may write

$$MR(H) = \exp(-\Delta E_a(H)/k_BT) - 1 = -\Delta E_a(H)/k_BT. \quad (6)$$

We have considered both the Langevin $\mathfrak{L}(x)$ and the Brillouin $\mathfrak{B}_J(x)$ functions, where $x = \mu_0 m_{eff} H/k_BT$ to simulate the $\Delta E_a(H)$ variations. The parameter m_{eff} is the total magnetic moment borne by an ideal domain with // Fe^{2+} and Fe^{3+} magnetic moments. We recall here that even at saturation, some spins in the film will show a deviation of their directions (spin canting) with respect to the field direction, due to the inherent presence of domain boundaries, composition variations, vacancies. The MR(H) data were found better fitted with the $\mathfrak{L}(x)$ function than with the $\mathfrak{B}_J(x)$ one. For both models, a linear variation with T of m_{eff} needs to be introduced, which probably reflects a temperature dependence of the tunneling barrier between adjacent domains. At 300 K, using the Langevin fit, one obtains $m_{eff} = 110\,\mu_B$ for the single oriented film and $295\,\mu_B$ for the polycrystalline film. This corresponds to 28 and 74 Fe^{2+} cations inside ideally magnetized zinc ferrite clusters of an average size equal to 12 and 31 nm, respectively. The MR(H) behaviors corroborate the result deduced from the M(T) curves that the ferromagnetic ordering of magnetic moments in the dense polycrystalline film is established on longer distances than in the (111) film.

IV. CONCLUSION

In summary, we have grown on different substrates, using a growth temperature of 500 °C and oxygen deficient conditions (10^{-7} mbar O_2), (111)- and (001)-oriented $Zn_xFe_{3-x}O_{4-y}$ films displaying long-range ferrimagnetic order and thermally activated charge transport properties. Among these films, the best quality ones are the (111)-oriented films obtained on SiO_2/Si substrates. One may reach 85% of the theoretical saturation magnetization (≈600 kAm^{-1} or 4.8 μ_B per f.u. at 10 K for the $x = 0.33$ film). *In situ* post-annealing of RT grown films leads to a high quality polycrystalline form with stoichiometric layers exempt of the APB defects inherent to the single-oriented growth. In this case, a remnant of the Verwey transition is identified both in the magnetization and charge transport measurements. While a very good

ferromagnetic behavior is preserved up to 300 K and the resistivity keeps lower than that of the as-grown single-oriented films, the MR presents novel specific features with respect to the single-oriented films: a more significant low field value (MR $\approx -$ 1.5% at 0.5 T) and near saturation behavior at high field. This suggests an improved spin-polarized transport. Such oxide films with optimized moment/charge ordering might be used in multilayer structures such as magnetic tunnel junctions, spin valves, and more generally in novel spintronics devices.

ACKNOWLEDGMENTS

The authors are indebted to D. Demaille for the TEM measurements. They thank M. Escudier, F. Breton, and L. Becerra for the technical support concerning clean room preparations, S. Hidki and W. Seiler for the XRD measurements, L. Thevenard and Y. Klein for their fruitful advices about the PPMS. The RBS experiments were performed under the Convention for SAFIR@ALTAÏS between the Université Pierre et Marie Curie and the University of Namur.

[1]M. Bibes, J. E. Villegas, and A. Barthelemy, Adv. Phys. **60**, 5 (2011).
[2]M. Opel, J. Phys. D: Appl. Phys. **45**, 033001 (2012).
[3]J.-B. Moussy, J. Phys. D: Appl. Phys. **46**, 143001 (2013).
[4]Z. Zhang and S. Satpathy, Phys. Rev. B **44**, 13319 (1991).
[5]Y. S. Dedkov, U. Rüdiger, and G. Güntherodt, Phys. Rev. B **65**, 064417 (2002).
[6]P. Wang, Z. Ka¸kol, M. Wittenauer, and J. M. Honig, Phys. Rev. B **42**, 4553 (1990).
[7]D. Venkateshvaran, M. Althammer, A. Nielsen, S. Geprägs, M. S. R. Rao, S. T. B. Goennenwein, M. Opel, and R. Gross, Phys. Rev. B **79**, 134405 (2009).
[8]J. Takaobushi, H. Tanaka, T. Kawai, S. Ueda, J.-J. Kim, M. Kobata, E. Ikenaga, M. Yabashi, K. Kobayashi, Y. Nishino, D. Miwa, K. Tamasaku, and T. Ishikawa, Appl. Phys. Lett. **89**, 242507 (2006).
[9]C. E. R. Torres, F. Golmar, M. Ziese, P. Esquinazi, and S. P. Heluani, Phys. Rev. B **84**, 064404 (2011).
[10]J. Robertson, Rep. Prog. Phys. **69**, 327 (2006).
[11]D. Reisinger, M. Schonecke, T. Brenninger, M. Opel, A. Erb, L. Alff, and R. Gross, J. Appl. Phys. **94**, 1857 (2003).
[12]S. M. Watts, K. Nakajima, S. van Dijken, and J. M. D. Coey, J. Appl. Phys. **95**, 7465 (2004).
[13]C. Boothman, A. M. Sánchez, and S. van Dijken, J. Appl. Phys. **101**, 123903 (2007).
[14]M. Monti, B. Santos, A. Mascaraque, O. Rodrıguez de la Fuente, M. A. Nino, T. O. Mentes, A. Locatelli, K. F. McCarty, J. F. Marco, and J. de la Figuera, Phys. Rev. B **85**, 020404(R) (2012).
[15]D. T. Margulies, F. T. Parker, M. L. Rudee, F. E. Spada, J. N. Chapman, P. R. Aitchison, and A. E. Berkowitz, Phys. Rev. Lett. **79**, 5162 (1997).
[16]S. Celotto, W. Eerenstein, and T. Hibma, Eur. Phys. J. B **36**, 271–279 (2003).
[17]W. Eerenstein, T. T. M. Palstra, T. Hibma, and S. Celotto, Phys. Rev. B **66**, 201101(R) (2002).
[18]S. Ueda, H. Tanaka, J. Takaobushi, E. Ikenaga, J. J. Kim, M. Kobata, T. Kawai, H. Osawa, N. Kawamura, M. Suzuki, and K. Kobayashi, Appl. Phys. Express **1**, 077003 (2008).
[19]D. Venkateshvaran, W. Kaiser, A. Boger, M. Althammer, M. S. R. Rao, S. T. B. Goennenwein, M. Opel, and R. Gross, Phys. Rev. B **78**, 092405 (2008).
[20]V. G. Harris, N. C. Koon, C. M. Williams, Q. Zhang, M. Abe, and J. P. Kirkland, Appl. Phys. Lett. **68**, 2082 (1996).
[21]Y. Li, Q. Li, M. Wen, Y. Zhang, Y. Zhai, Z. Xie, F. Xu, and S. Wei, J. Electron. Spectrosc. Relat. Phenom. **160**, 1 (2007).
[22]J. P. Shepherd, R. Aragón, J. W. Koenitzer, and J. M. Honig, Phys. Rev. B **32**, 1818 (1985).
[23]M. Ziese, R. Höhne, H. C. Semmelhack, H. Reckentin, N. H. Hong, and P. Esquinazi, Eur. Phys. J. B **28**, 415 (2002).
[24]S. I. Rybchenko, Y. Fujishiro, H. Takagi, and M. Awano, Phys. Rev. B **72**, 054424 (2005).
[25]P. Chen, D. Y. Xing, Y. W. Du, J. M. Zhu, and D. Feng, Phys. Rev. Lett. **87**, 107202 (2001).
[26]H.-C. Wu, M. Abid, B. S. Chun, R. Ramos, O. N. Mryasov, and I. Shvets, Nano Lett. **10**, 1132 (2010).